

REFERENCES AND NOTES

- R. Thom, L. Moore, W. D. Sproul, T. P. Chang, *Surf. Coat. Technol.* **62**, 423 (1993).
- U. Helmersson *et al.*, *J. Appl. Phys.* **62**, 481 (1987).
- M. Shinn, L. Hultman, S. A. Barnett, *J. Mater. Res.* **7**, 901 (1992).
- W. D. Sproul, P. J. Rudnik, M. E. Graham, S. L. Rohde, *Surf. Coat. Technol.* **43/44**, 270 (1990).
- W. D. Sproul, P. J. Rudnik, M. E. Graham, C. A. Gogol, R. M. Mueller, *ibid.* **39/40**, 499 (1989).
- X. Chu, M. S. Wong, W. D. Sproul, S. L. Rohde, S. A. Barnett, *J. Vac. Sci. Technol. A* **10**, 1604 (1992).
- X. Chu, S. A. Barnett, M. S. Wong, W. D. Sproul, *Surf. Coat. Technol.* **57**, 13 (1993).
- P. B. Mirkarimi, thesis, Northwestern University, Evanston, IL (1993); ———, L. Hultman, S. A. Barnett, *Appl. Phys. Lett.* **57**, 2654 (1990).
- M. Shinn and S. A. Barnett, *Appl. Phys. Lett.* **64**, 61 (1994).
- X. Chu, thesis, Northwestern University, Evanston, IL (1995).
- W. M. C. Yang, T. Tsakalagos, J. E. Hilliard, *J. Appl. Phys.* **48**, 876 (1977); S. A. Barnett and N. Yao, in *Physics of Thin Films*, J. L. Vossen and M. Francombe, Eds. (Academic Press, New York, 1993), vol. 17, pp. 1–77.
- X. Chu and S. A. Barnett, *J. Appl. Phys.* **77**, 4403 (1995).
- S. Schiller *et al.*, *Surf. Coat. Technol.* **61**, 331 (1993); P. Frach, U. Heisig, Chr. Gottfried, H. Walde, *ibid.* **59**, 177 (1993); M. E. Graham and W. D. Sproul, in *37th Annual Technical Conference Proceedings* (Society of Vacuum Coaters, Albuquerque, NM, 1994), pp. 275–279; W. D. Sproul *et al.*, *J. Vac. Sci. Technol. A* **13**, 1188 (1995); S. Schiller, K. Goedicke, V. Kirhhoff, T. Kopte, in *38th Annual Technical Proceedings* (Society of Vacuum Coaters, Albuquerque, NM, 1995), pp. 293–297.
- J. Sellers, "Asymmetric Bipolar Pulsed DC," *ENI Tech. Note* (ENI, Division of Astec America, Rochester, NY, 1995).
- J. M. Schneider, W. J. Chia, J. Rechner, W. D. Sproul, M.-S. Wong, in preparation.
- M.-S. Wong *et al.*, *Surf. Coat. Technol.*, in press.
- The polycrystalline nitride superlattice work was sponsored by the U.S. Department of Energy, Division of Materials Sciences, Office of Basic Energy Science, grant DE-FG02-926ER45434. The oxide superlattice work is being sponsored by the U.S. Air Force Office of Scientific Research, grant F49620-95-0177.

Biomimetic Pathways for Assembling Inorganic Thin Films

I. A. Aksay, M. Trau, S. Manne, I. Honma, N. Yao, L. Zhou, P. Fenter, P. M. Eisenberger, S. M. Gruner

Living organisms construct various forms of laminated nanocomposites through directed nucleation and growth of inorganics at self-assembled organic templates at temperatures below 100°C and in aqueous solutions. Recent research has focused on the use of functionalized organic surfaces to form continuous thin films of single-phase ceramics. Continuous thin films of mesostructured silicates have also been formed on hydrophobic and hydrophilic surfaces through a two-step mechanism. First, under acidic conditions, surfactant micellar structures are self-assembled at the solid/liquid interface, and second, inorganic precursors condense to form an inorganic-organic nanocomposite. Epitaxial coordination of adsorbed surfactant tubules is observed on mica and graphite substrates, whereas a random arrangement is observed on amorphous silica. The ability to process ceramic-organic nanocomposite films by these methods provides new technological opportunities.

Biologically produced inorganic-organic composites such as bone, teeth, diatoms, and sea shells are fabricated through highly coupled (and often concurrent) synthesis and assembly. These structures are formed through template-assisted self-assembly, in which self-assembled organic material (such as proteins, or lipids, or both) form the structural scaffolding for the deposition of inorganic material (1). They are hierarchically structured composites in which soft organic materials are organized on length

scales of 1 to 100 nm and used as frameworks for specifically oriented and shaped inorganic crystals (that is, ceramics such as hydroxyapatite, CaCO₃, SiO₂, and Fe₃O₄) (1–3). In some cases, structurally organized organic surfaces catalytically or epitaxially induce growth of specifically oriented inorganic thin films. Most importantly, however, nature's way of mineralization uses environmentally balanced aqueous solution chemistries at temperatures below 100°C. This approach provides an attractive alternative to the processing of inorganic thin films, especially in applications where substrates cannot be exposed to high temperatures, or more generally in the pursuit of increased energy efficiency.

A classic and a widely studied example of a biocomposite is the nacre of abalone

shell, in which thin films of organic (<10 nm) and inorganic (<0.5 μm) phases are coupled together to produce a laminated structure with improved mechanical properties (4–6). Scanning electron microscopy (SEM) and transmission electron microscopy (TEM) images of this material are shown in Fig. 1. Because of this special architecture, composites such as nacre are simultaneously hard, strong, and tough (4–6). The core of the organic template is composed of a layer of β-chitin layered between "silk-like" glycine- and alanine-rich proteins (7). The outer surfaces of the template are coated with hydrophilic acidic macromolecules rich in aspartic and glutamic acids (8). Recent studies suggest that these acidic macromolecules alone are responsible for control of the polymorphic form and the morphology of the CaCO₃ (calcite versus aragonite) crystals (9), although the role of the β-chitin supported matrix on the lamellar morphology of the CaCO₃ layers over macroscopic dimensions still remains to be determined. Morphological and crystallographic analyses of the aragonitic thin layers of nacre by electron microdiffraction show that c-axis-oriented aragonite platelets form a hierarchical tiling of a twin-related dense film with twin domains extending over three length scales (4, 10). Superposition of the aragonite lattices on all three possible sets of twins generates a new superlattice structure, which suggests

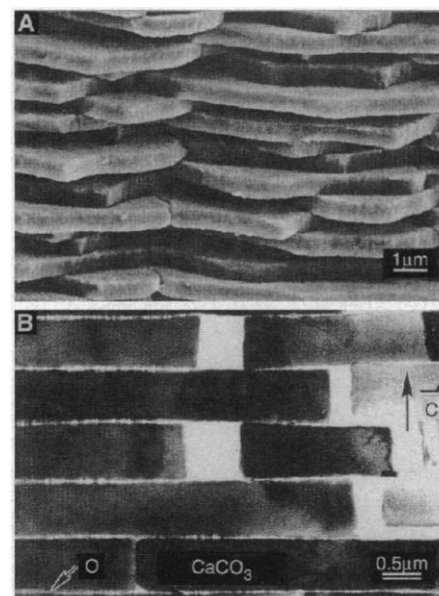


Fig. 1. (A) An SEM (Philips XL30FEG) image of fracture surface of abalone nacre showing aragonite (CaCO₃) platelets of ~0.5 μm thick. (B) A TEM (Philips CM200) image of the nacre cross section revealing a <10 nm thin organic film (marked "O") between the aragonite platelets with their c-axis normal to the organic template.

The authors are at Princeton University, Princeton, NJ 08544-5263, USA. I. A. Aksay, M. Trau, and I. Honma are in the Department of Chemical Engineering and the Princeton Materials Institute; S. Manne and N. Yao are in the Princeton Materials Institute; and L. Zhou, P. Fenter, P. M. Eisenberger, and S. M. Gruner are in the Department of Physics and the Princeton Materials Institute.

that the organic template adopts a single-crystalline pseudohexagonal structure (10). Although cellular activities leading to the self-assembly of the organic template remain to be understood, the presence of an organized organic template is essential to the assembly of the inorganic layer.

Nature's way of processing such hierarchically structured composite materials with designed architecture is an invaluable guide to developing new synthetic processes that can produce useful materials with similar designs. Toward this goal, several key aspects of the biomineralization scheme need to be understood. The first key aspect is the mechanism leading to the self-assembly of an organized organic template and choice of organics to form a desired inorganic. Second, the orienting and shaping action of the assembled organic scaffolding on the growing inorganic phase needs to be elucidated, as does the oriented assembly of organics on the deposited inorganic substrates. Third, the controlled nucleation and growth of inorganic material in specific sites, and finally, the assembly of higher order hierarchical structures and the role of hierarchical architecture on property optimization require explanation. Given the demand for ceramic coatings with enhanced optical, magnetic, electronic, mechanical, and "intelligent" functions (11), a detailed study of biomimetic film formation will not only have important technological impact but will also shed light on the fundamental processes listed above.

Synthetic Pathways

All mineralization processes involve the precipitation of inorganic material from solution. A key requirement for successful film formation is to promote the formation of the inorganic phase on the substrate directly (that is, heterogeneous nucleation) and prevent the homogeneous nucleation of particles in the solution (11). According to classical nucleation theory (12), the free energy change (ΔF) associated with the precipitation of an inorganic cluster from solution onto a surface is given by:

$$\Delta F = -nk_B T \ln S + \gamma_{il}A_{il} + (\gamma_{is} - \gamma_{sl})A_{is} \quad (1)$$

where S represents the degree of supersaturation in the fluid; n is the aggregation number; k_B is Boltzmann's constant; T is temperature; γ_{il} , γ_{is} , and γ_{sl} represent the inorganic/liquid, inorganic/substrate, and substrate/liquid interfacial tension, respectively; and A_{il} and A_{is} represent the corresponding interfacial areas. When the interaction between the growing nucleus and substrate surface represents a lower net interfacial energy than the inorganic/solution

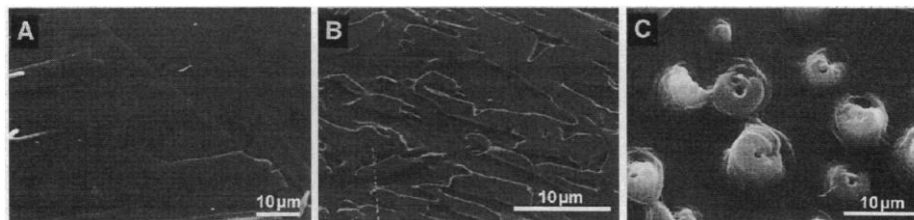


Fig. 2. SEM images of mesoscopic silica films grown at (A) mica/water, (B) graphite/water, and (C) silica/water interface for 24 hours, respectively. Oriented tapes are observed on mica and graphite. The films grown at the silica/water interface are uniform initially (dark background) but spiral-like structures (light features) form later.

interfacial energy [that is, $(\gamma_{is} - \gamma_{sl})A_{is} < \gamma_{il}A_{il}$], heterogeneous nucleation is favored over homogeneous nucleation. This is the case for the majority of precipitating inorganic systems, and hence heterogeneous nucleation is the dominant precipitation mechanism for thermodynamically controlled systems. Homogeneous nucleation will only dominate at relatively high levels of supersaturation where the precipitation process becomes kinetically controlled. Precipitation times for homogeneous nucleation vary enormously, from months to milliseconds, depending sensitively on the value of S (13). Thus, an important requirement for the biomimetic processing of thin inorganic films is to maintain relatively low levels of supersaturation during the precipitation process in order to minimize the amount of particle formation in bulk solution.

In recent years, a substantial number of researchers have demonstrated the viability of this approach for the preferential growth of inorganic crystals at the solid/liquid (11, 14) and liquid/air interfaces (15). Furthermore, through chemical modification of these interfaces, by adsorbing surfactants or other reactive moieties, the crystal phase, morphology, growth habit, and even chirality of heterogeneously deposited inorganics can be controlled. Innovative examples of this approach include the work of Mann *et al.* (16), where phase-specific, oriented calcite crystals are grown underneath a compressed surfactant monolayer at the air/water interface. Changing surfactant type or degree of monolayer compression results in different crystal phases and orientations. Another innovative approach is that of the Pacific Northwest National Laboratories (PNNL) (11). By chemically modifying solid metal, plastic, and oxide surfaces, these researchers have demonstrated selection of phase and orientation of the depositing crystalline inorganic at a variety of solid/liquid interfaces. A particularly attractive strategy is the use of the self-assembled monolayer (SAM) approach to coat metal and oxide substrates with surfactant monolayers of tailored hydrophilicity. This is accomplished by pretreating the substrates

with a solution of functionalized surfactants, such as sulfonic acid-terminated octadecyl trichlorosilane, before precipitation of the inorganic phase. The choice of the terminating moiety on the surfactant tail determines surface charge and relative hydrophobicity of the chemisorbed surfactant monolayer. In this way, oxide and metal (17) substrates can be modified conveniently to have the required surface properties to promote inorganic film growth.

Potential applications for dense, polycrystalline inorganic films span a broad range of industries. These include the possibility of applying hard optical coatings to plastics in order to replace glass, abrasion-resistant coatings for plastic and metal components subject to wear, and the deposition of oriented films of iron oxide phases for use as magnetic storage media. For many of the above applications, conventional ceramic processing methods, which require high-temperature sintering, cannot be used because of problems with substrate degradation. A significant advantage of the biomimetic processing methods described above is the relatively low processing temperatures involved (typically $<100^\circ\text{C}$) and the use of water rather than organic solvents (11). Both of these factors render such methods relatively environmentally benign.

Whitesides' group at Harvard University (18) has developed a microcontact printing method by which complex, designed SAM patterns may be transferred onto substrates with an elastomeric stamp. This approach sets up lateral variations in the $\gamma_{is} - \gamma_{sl}$ value along the substrate and may be used to selectively nucleate and grow inorganic phase on the functionalized regions. The PNNL group (19) has demonstrated the spatially resolved deposition of FeOOH mineral through an analogous SAM approach by using electron and ion beam lithography to pattern the SAM layer. This technique allows micrometer-scaled patterning of inorganic materials on a variety of substrates through confined nucleation and growth of inorganic films. Similar work has recently been reported by the Case Western Reserve University group (20, 21), where photoli-

thography was used to pattern the SAM layer prior to area-selective mineralization of TiO_2 , ZrO_2 , SiO_2 , or Y_2O_3 films. An alternative to the SAM approach is the method of micromolding in capillaries (MIMIC) developed by Kim *et al.* (22). In this case, submicrometer-scale patterning of inorganic films is achieved by placing an elastomeric stamp, containing relief features on its surface, into contact with a substrate. Contact between the elastomeric stamp and the substrate forms a network of interconnected channels that may be filled with an inorganic precursor fluid [such as poly(ethoxymethylsiloxane)] through capillary action. After the material in the fluid is cross-linked, crystallized, or deposited onto the substrate, the elastomeric stamp is removed to leave behind a patterned inorganic film with microstructures complementary to those present in the mold.

The above techniques represent advances in the selective nucleation and growth of inorganic crystals with specific phase, orientation, and micropatterns. However, once the inorganic layer begins to grow away from the substrate/solution interface, there is no facility for organic material to adsorb onto or to become incorporated within the growing inorganic structure or to do both, as in the case of nacre. The deliberate and designed fabrication of hierarchically structured materials built by multilayering of self-assembled nanocomposite films has not been explored. In learning from nature, our goal is to build exactly these types of composite materials rather than single-phase inorganics.

Template-Assisted Thin Films Through Surfactant Self-Assembly

The synthesis of silica-based mesostructured materials (23) by using supramolecular assemblies of surfactant molecules to template the condensation of inorganic species has attracted considerable interest as a biomimetic approach to the fabrication of organic/inorganic nanocomposites. This synthesis scheme has now been extended to include a wide variety of transition metal oxides (24) and, recently, to cadmium sulfide and selenide semiconductors (25). Although the exact mechanism for this type of mineralization is still controversial (26), this technique holds great promise as a synthetic scheme to produce nanostructured materials with novel properties. For any of these applications to be realized, however, what is required is a method by which these nanostructures can be formed into controlled shapes and patterns rather than the microscopic particulates that have been previously reported.

One approach has been to start with a well-defined interface such as mica, as recently illustrated by Yang *et al.* (27). Under acidic conditions, reactive SiOH anchoring sites on mica are assumed to provide binding sites for the silica-surfactant micellar precursor species and orient a hexagonal phase of mesostructured silica as a continuous thin film. Our work has shown that this approach is not just limited to the hydrophilic surface of mica but can be generalized to form continuous mesostructured silicate films onto a wide variety of substrates, including hydrophobic surfaces such

as graphite. The mechanism of film formation is also revealed through atomic force microscope (AFM) analysis of the growing films. Of primary concern here is the structure of the first layer of adsorbed surfactant at each of these interfaces. Although the molecular organization and self-assembly of surfactants at interfaces is a widely studied area, little is still known about the precise structure of adsorbed surfactant layers. Recent work (28) has shown that three-dimensional surfactant structures such as cylindrical tubules and spheres can be formed at solid/liquid interfaces. Adsorbed hemimicellar arrangements are observed on poorly orienting amorphous substrates, such as silica, and aligned tubular structures are observed on more strongly orienting crystalline substrates such as mica and graphite. The latter substrates orient adsorbed surfactants through anisotropic attraction (either van der Waals or electrostatic) between the crystalline substrate and the surfactant molecule. The amorphous silica substrate has no preferential orientation for surfactant adsorption.

In order to promote growth of a mesostructured inorganic on these substrates, an aqueous recipe that includes an excess of adsorbing cetyltrimethyl ammonium chloride (CTAC) surfactant and a dilute acidic solution of tetraethoxy silane (TEOS) inorganic precursor is used. Inorganic solute concentrations are purposefully kept dilute in order to decrease the rate of homogeneous nucleation to such an extent that the more thermodynamically favored heterogeneous nucleation route is dominant (29).

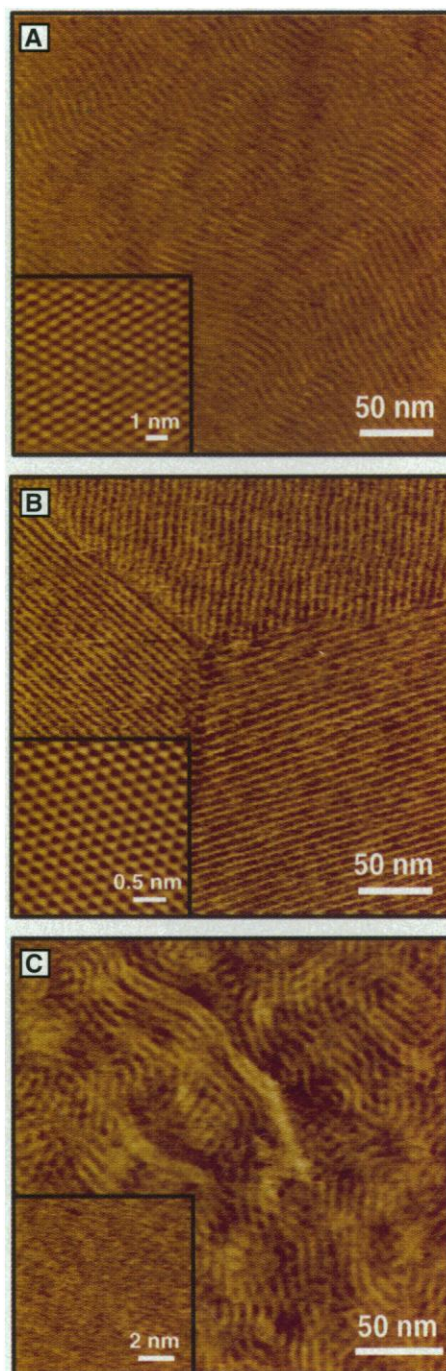


Fig. 3. In situ AFM images of mesostructured films growing on mica, graphite, and amorphous silica substrates, respectively. AFM images of the mica, graphite, and silica substrates used to grow mesoscopic silica films are shown in the insets. (A) and (B) illustrate the periodic mica and graphite atomic lattices, respectively, onto which CTAC adsorbs and orients; (C) reveals a smooth, amorphous silica substrate. Images of the films were obtained in "noncontact" mode, utilizing the electrical double layer force described in (28, 31). (A) Meandering surfactant tubules on the mica substrate, 6.2 to 6.8 nm spacing, oriented parallel to the solid/liquid interface. Tubules are initially aligned along one of the three next-nearest-neighbor directions of the mica oxygen lattice displayed in inset. In the early stages of the reaction (<7 hours), this orientation is preserved as tubules continue to assemble and grow away from the interface coupled with silica polymerization. (B) On graphite, tubules align parallel to the substrate along one of three symmetry axes of the hexagonal carbon lattice shown in the inset. Unlike the structures on mica, these do not meander but form rigid parallel stripes. (C) On amorphous silica, periodic dimples are observed rather than stripes, suggesting an orientation of the tubules away from the interface.

Figure 2 shows SEM images of mesoscopic films grown for a period of 24 hours at the mica, graphite, and silica/water interfaces (30). All of the films are continuous and display distinctly different textures at length scales between 0.5 and 10 μm . Figure 3 shows in situ AFM images of the atomic lattice of each substrate as well as the structure of the mesoscopic silica overlayer growing on each surface (31, 32).

In the case of mica, Fig. 3A reveals meandering stripes with a spacing of 6.2 to 6.8 nm. These are observed at every stage of the reaction (33). As discussed below, x-ray diffraction (XRD) analysis of these films reveals a distorted hexagonal stacking of surfactant tubules (5.6 nm nearest-neighbor spacing) that lie parallel to the

surface and are axially aligned along the next-nearest-neighbor direction of the hexagonal oxygen lattice on the mica surface. Figure 4 shows TEM images of a mesostructured film on mica, cut in two different transverse directions. All three methods reveal a consistent structure of the mesostructured film on mica. AFM images similar to those in Fig. 3A were obtained without TEOS present, but these interfacial surfactant films are limited to one or two layers of cylindrical tubules (34). The self-assembly of micellar layers without the presence of the inorganic agent suggests a sequential growth and polymerization for the silicate films (Fig. 5A). First, the surfactant self-assembles on the mica substrate to form meandering tubules, and second, silicon hy-

droxide monomers (or multimers) polymerize at the micellar surface. As polymerization continues, more surfactant is adsorbed to the freshly formed inorganic surface and allows the templated mesoscopic structure to replicate itself and grow in to the bulk solution. After growth periods of 24 hours, the mesoscopic composite films begin to develop larger scale structural features such as those shown in Fig. 2A. At this stage, aligned "tapes" and steps appear with macroscopic grain boundary angles of 60° and 120° . These macroscopic angles clearly result from atomic level registry of the surfactant tubules with the underlying mica lattice.

For graphite substrates (Figs. 2B and 3B), the surfactant tubules are also aligned parallel to the surface, but in this case they are rigid, parallel stripes without the meandering curvature observed on mica. Measured nearest-neighbor spacings similar to that seen on mica and microscopic grain boundaries can be clearly imaged, which again suggests a preferential axial orientation of the surfactant tubules with the hexagonal graphite lattice. The graphite surface is distinct from mica in that it is hydrophobic and does not contain ionizable moieties to engender surface charge. Attractive interactions (hydrophobic and van der Waals) between the graphite surface and surfactant tails cause them to adsorb horizontally (Fig. 5B), and the resulting large interaction area

Fig. 4. TEM images of a mesostructured silica film grown on mica. Both images are in a transverse orientation with respect to the film and reveal hexagonal packing of tubules aligned parallel to the substrate. The image in (A) reveals a slight elliptical distortion of the tubules suggesting that the films are strained, that is, compressed in the direction normal to the template.

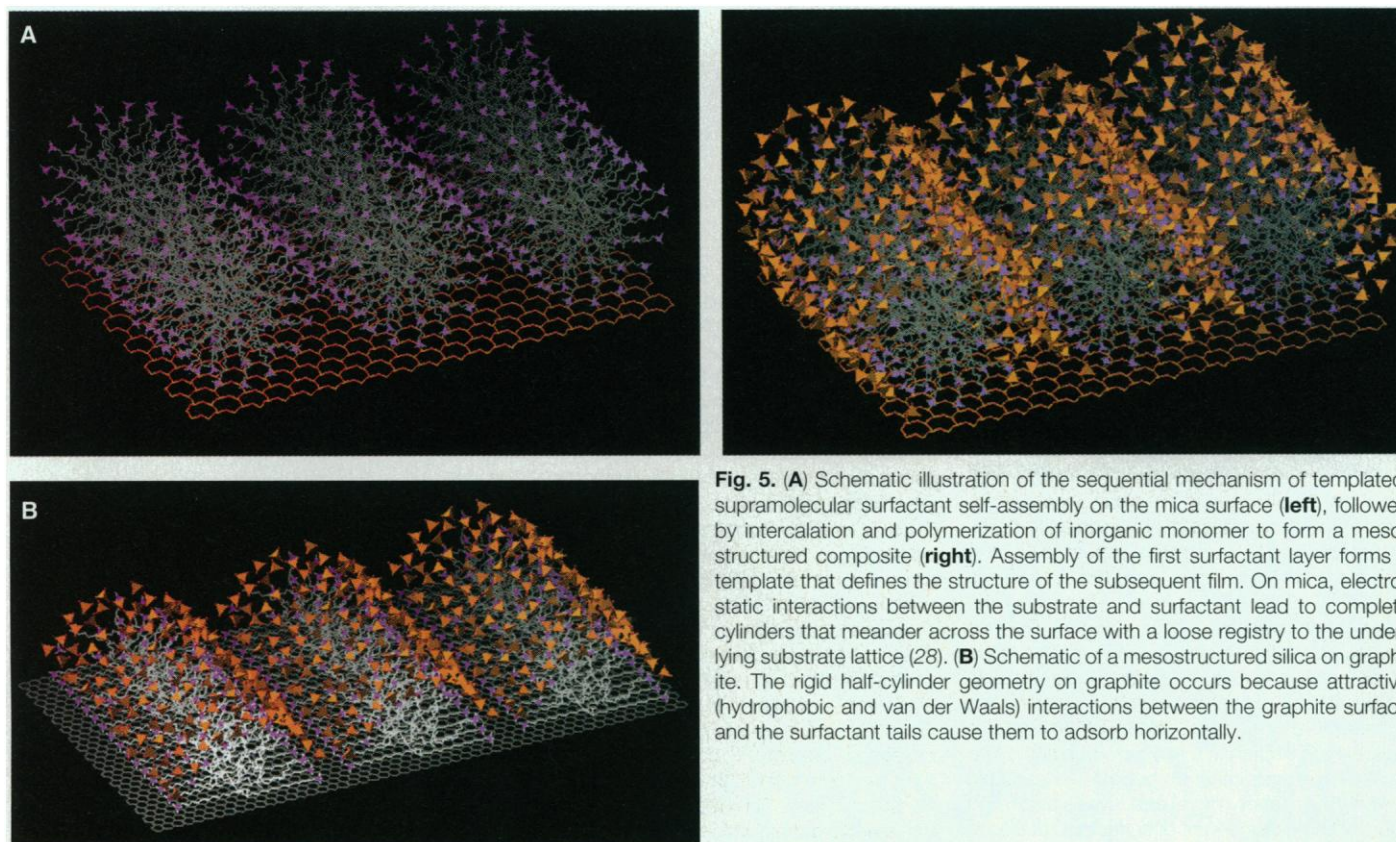
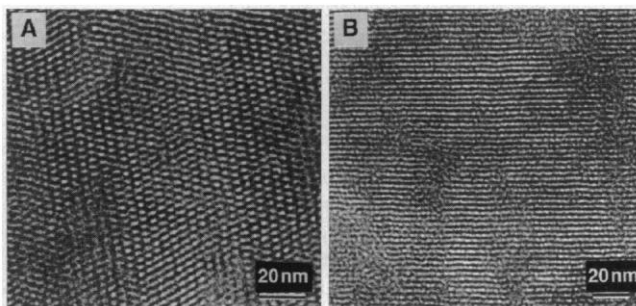


Fig. 5. (A) Schematic illustration of the sequential mechanism of templated, supramolecular surfactant self-assembly on the mica surface (left), followed by intercalation and polymerization of inorganic monomer to form a mesostructured composite (right). Assembly of the first surfactant layer forms a template that defines the structure of the subsequent film. On mica, electrostatic interactions between the substrate and surfactant lead to complete cylinders that meander across the surface with a loose registry to the underlying substrate lattice (28). (B) Schematic of a mesostructured silica on graphite. The rigid half-cylinder geometry on graphite occurs because attractive (hydrophobic and van der Waals) interactions between the graphite surface and the surfactant tails cause them to adsorb horizontally.

per molecule gives rise to a strong orientation effect between molecule and substrate (28) that is preserved in the cylindrical aggregates. Mica interacts only with the head group (28) and orients the adsorbed molecules vertically; the smaller interaction area gives rise to a correspondingly smaller orientation effect. At long reaction times, macroscopic features grow out of the oriented, uniform film similar to those seen on mica. As with mica, edges with macroscopic angles of 60° and 120° are also observed.

Growth of these films at the silica/water interface gives rise to silica films with macro- and microstructures dramatically different from the ones described above. Figure 3C shows an in situ AFM image of the reacting film grown from a silica substrate. Rather than the parallel stripes observed on the previous

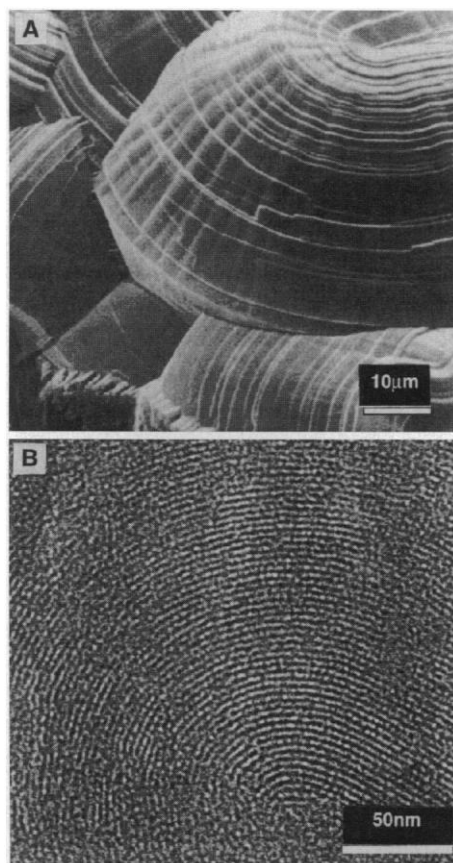


Fig. 6. (A) An SEM image of a hierarchically structured mesoscopic silica film grown on a silica substrate. Although all of the films appear uniform at early stages of the reaction, once film thicknesses exceed $\sim 0.5 \mu\text{m}$, the ordering influence of the substrate becomes no longer important. Release of accumulated strain energy within the film leads to hierarchical structures, with tubule bundles wrapping around each other in three dimensions on several length scales. (B) A TEM image of a planar cross section of a film grown on silica. The cross section was taken through a macroscopic swirl in the film shown in (A) and reveals a spiraling and twisting arrangement of surfactant tubules.

substrates, this image shows periodic arrays of dimples suggesting an orientation of surfactant tubules out of the plane of the interface. An XRD analysis confirms a distorted hexagonal packing of the tubules. The dimpled pattern suggests a twisting arrangement of hexagonally packed tubules attached to the interface at one end and spiraling into the solution. Similar dimpled structures were also observed with neat CTAC solution, which suggests the formation of roughly spherical surfactant aggregates that act as starting points on the surface for growth of cylindrical tubules into the solution. Micellar structures of quaternary ammonium surfactants on silica have been previously postulated and observed by other workers (28, 35).

As in the case of mica and graphite, the structure formed in the silica substrate films is a direct consequence of the arrangement of the first layer of adsorbed surfactant on the surface. It appears that the ordering ability of the silica interface, which is dramatically different from that of mica and graphite, is not great enough to confine the surfactant tubules to lie straight on planar surfaces. Indeed, having nucleated one end of the tubules at the interface, the long axes of the tubules appear to wander over a wide range of slowly curving configurations in three dimensions, suggesting that it takes very little energy to bend the tubules along their long axes. This effect may simply be understood in terms of a Helfrich (36) bending energy model of the tubule surfactant layer:

$$E = \frac{k_c}{2} \left(\frac{1}{R_1} + \frac{1}{R_2} - \frac{1}{R_0} \right)^2 + \frac{k_g}{R_1 R_2} \quad (2)$$

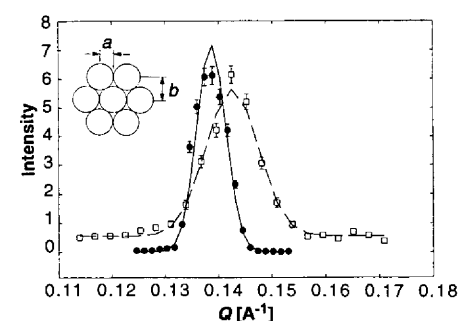
where E is the free energy per unit area

(effectively, an energy per surfactant molecule); k_c and k_g are the rigidity and Gaussian curvature constants, respectively; and R_1 , R_2 , and R_0 are the principal radii and the spontaneous radius of curvature, respectively. Although this form was derived for the thin-film limit in which the radii are large compared to the thickness of the surfactant layer, it also appears to describe reasonably well certain cases in which the surfactant layer thickness is comparable to R_1 and R_0 (37). R_1 , the small radius of the tubule, is strongly constrained by the length of the surfactant molecules. Insofar as R_0 is fixed by the surfactant composition and is small ($\sim 5 \text{ nm}$), as is typically the case for single-chain surfactants, and if $R_2 \gg R_1$, as is the case for long, thin tubules, then Eq. 2 is well approximated by:

$$E = k_c/2(1/R_1 - 1/R_0)^2 \quad (3)$$

In other words, the energy of bending along the long axis of a tubule does not figure prominently into the bending energy. Unless order is imposed on the tubules by external forces, such as adsorption forces, the tubules will sample a wide range of slowly varying configurations. This prediction is also consistent with observed macroscopic structures of mesoscopic silica films formed after long growth times at the silica/water interface (Fig. 6). These films begin growing as very uniform structures but soon become increasingly textured and chaotic as the film thickness increases. Rather than the oriented tapes observed in the cases of mica and graphite substrates, the silica substrate films display chaotic, spiral-like structures wrapped in a hierarchical fashion around each other

Fig. 7. Grazing angle of incidence XRD data for a mesostructured silica film growing at the mica/ aqueous solution phase interface (after 15 hours of reaction time) showing radial scans of two Bragg peaks, the (002) (filled circles) and the (101) (open squares, expanded by a factor of 1350). Growth of the surfactant film on a freshly cleaved mica substrate results in a highly aligned crystalline lattice, in which the (002) Bragg peak is oriented along the substrate surface normal, with a mosaic width that is less than 0.06° . Furthermore, the (101) Bragg peak is also azimuthally aligned within the surface plane, such that the tubules are oriented along the next-nearest-neighbor direction of the surface oxygen lattice, and having an in-plane mosaic width of $\sim 10^\circ$. Both of these observations clearly suggest that the substrate has a strong orienting effect on the co-assembled film. Further evidence of the interaction between the substrate and the co-assembled film can be found in the exact Bragg peak positions. Although bulk mesoscopic silica exhibits a hexagonal lattice (23, 26), in which case $Q_{002} = Q_{101}$, for films grown on mica the radial peak position of the (002) and (101) Bragg peaks are not equal ($Q_{002} = 0.139 \text{ \AA}^{-1}$ and $Q_{101} = 0.143 \text{ \AA}^{-1}$), which implies that the film is strained. From these data, we derive nearest-neighbor spacings of 52 and 50 Å. This strain results in a ratio of lattice spacings of $b/a = 1.80$, as compared with the expected hexagonal value of $\sqrt{3}$, corresponding to a strain of $\delta_n = (b/\sqrt{3}a) - 1 = 3.7\%$, and an area per tube in the composite film of 2288 \AA^2 (the inset defines the parameters a and b , and the lines show the model fit). Strain in these films results from epitaxial mismatch between the first adsorbed surfactant layer and the periodic atomic lattice of the substrate.



(Figs. 2C, 3C, and 6). The films become increasingly disordered once the thickness is great enough such that the surface can no longer induce ordering.

Hierarchical Structures

To investigate the substrate ordering effect on surfactant tubules and subsequent mesoscopic silica films, we performed XRD analyses of films grown on mica. In these measurements, we terminate the growth by partially draining the solution in a sealed cell and perform the measurements while the sample is in contact with the vapor of the growth solution. Figure 7 indicates that the films are strained in the plane perpendicular to the substrate, with the hexagonal packing of tubules distorted by as much as 4% during growth. Upon drying, strain within the film is significantly altered (38). During growth, the strain appears to result from the ordering influence that the mica substrate exerts on the adsorbed surfactant tubules. That is, the forces that act to align the tubules parallel to the surface also act to deform the hexagonal packing in three dimensions. The forces responsible could be either van der Waals or electrostatic in nature because the mica surface has ionizable moieties. As the self-assembled organic layers grow away from the surface, the ordering effect is expected to diminish. Experiments performed in the absence of the TEOS inorganic precursor reveal that one or two layers of surfactant tubules can adsorb to the substrate prior to silica condensation (34). Once the TEOS is included in the solution, silica begins to condense within the adsorbed surfactant layers and films grow away from the surface. More layers of surfactant can now adsorb to the freshly formed silica interface, which provides a mechanism for the film to continue to grow out into the solution. This growth mechanism, however, does not relieve the original strain in the film. Moreover, as the film grows thicker, tubules adsorbed to the mesostructured silica will be strained differently to the initial layers adsorbed on the mica surface. Evidence for the eventual release of this strain is seen most clearly on the surface of films grown for long periods. An example is seen in Fig. 2A, where macroscopic features such as the "swirling tube" and "hook" appear and grow out of the aligned film in a wormlike manner. On mica, these features begin to occur at film thicknesses of ~ 0.5 μm and always possess a wormlike structure. For films grown at the silica/water interface, dramatically different structures are seen to grow out of the film at similar film thicknesses (Figs. 2C and 6). Although the first layer of tubule structure is different for each substrate, the release of accumulated strain

within these films through the growth of tubule bundles away from the oriented film is a common feature of all of these films. For mica and graphite, these bundles form wormlike structures, and for silica, tapes and spirals are formed that wrap around each other in a hierarchical manner. The hierarchical structures formed in thick films thus appear to result from the release of accumulated strain energy associated with the epitaxial mismatch between the first layer of adsorbed surfactant and the periodic atomic lattice of the substrate. In all cases, this is observed to occur only for relatively thick films (≥ 0.5 μm) where the ordering influence of the substrate no longer exists.

Summary

The understanding of biomineralization processes can lead to innovative approaches to materials synthesis. The strategy of manipulating macroscopic material properties through hierarchical control of composite microstructure is an important lesson for the materials engineer from biology. In order to create hierarchical composite structures, novel synthetic pathways are required. One of these pathways is the lamination of organic and inorganic thin films to create structures similar to those observed in nacre. We have surveyed a variety of techniques that attempt to control the phase, orientation, and microstructure of inorganic films precipitated at interfaces. Although the future of biomimetic processing encompasses the fabrication of bulk composites as well as thin films, we have focused our attention on film processing primarily to enable a fundamental understanding of the templating interactions that occur at the organic/inorganic interface. Another reason to concentrate on thin films is their numerous technological applications.

As a viable method for the production of thin composite films with designed nanoscaled architecture, we have presented a technique that uses the supramolecular assembly of surfactant molecules at interfaces to template the condensation of an inorganic silica lattice. In this manner, continuous mesostructured silica films can be grown on many substrates, with the corresponding porous nanostructure determined by the specifics of the substrate surfactant interaction. XRD analysis has revealed epitaxial alignment of the adsorbed surfactant layer with crystalline mica and graphite substrates, and significant strain in the mesostructured silica overlayer has also been measured. As films grow thicker, accumulated strain is released resulting in the growth of hierarchical structures from the ordered film. This scheme of mesostructured film synthesis with control of structural features over several length scales is a novel general

approach to the synthesis of inorganic composites with designed architecture at the nanometer-size scale. We envision that this technique will become a useful synthetic tool for the convenient and economic manufacture of biomimetic thin films for a wide variety of applications, especially when the method is extended to compositions other than silica and also to form patterns and complex shapes.

REFERENCES AND NOTES

1. H. A. Lowenstam and S. Weiner, *On Biomineralization* (Oxford Univ. Press, Oxford, 1989); *Biomineralization: Chemical and Biochemical Perspectives*, S. Mann, J. Webb, R. J. P. Williams, Eds. (VCH Press, New York, 1989).
2. *Hierarchically Structured Materials*, I. A. Aksay et al., Eds., *MRS Proc.* **255** (1992); *Hierarchical Structures in Biology as a Guide for New Materials Technology*, NMA464 (National Academy Press, Washington, DC, 1994).
3. S. Mann, *Nature* **365**, 499 (1993); B. R. Heywood and S. Mann, *Langmuir* **8**, 1492 (1992); S. Mann, *J. Chem. Soc. Dalton Trans.* **1993**, 1 (1993).
4. M. Sarikaya and I. A. Aksay, in *Structure, Cellular Synthesis and Assembly of Biopolymers*, S. T. Case, Ed. (Springer-Verlag, New York, 1992), pp. 1–25.
5. J. D. Currey, *Proc. R. Soc. London Ser. B* **196**, 443 (1977).
6. S. A. Wainwright et al., *Mechanical Design in Organisms* (Princeton Univ. Press, Princeton, NJ, 1982).
7. H. Nakahara and M. Kakei, *Bull. Yosai Dent. Univ.* **12**, 1 (1983); S. Weiner and W. Traub, *Philos. Trans. R. Soc. London Ser. B* **304**, 421 (1984); *FEBS Lett.* **111**, 311 (1980); S. Weiner, Y. Talmon, W. Traub, *Int. J. Biol. Macromol.* **5**, 325 (1983).
8. H. Nakahara, M. Kakei, G. Bevelander, *Jpn. J. Malacol.* **39**, 167 (1980); M. Cariolu and D. E. Morse, *J. Comp. Biol.* **157**, 717 (1988); J. Keith et al., *Comp. Biochem. Physiol.* **105**, 487 (1993); R. Humbert et al., *MRS Symp. Proc.* **330**, 89 (1994).
9. G. Falini et al., *Science* **271**, 67 (1996); A. M. Belcher et al., *Nature* **381**, 56 (1996).
10. M. Sarikaya, J. Liu, I. A. Aksay, in *Biomimetics: Design and Processing of Materials*, M. Sarikaya and I. A. Aksay, Eds. (AIP Press, Woodbury, NY, 1995), pp. 35–90.
11. B. C. Bunker et al., *Science* **264**, 48 (1994).
12. A. W. Adamson, *Physical Chemistry of Surfaces* (Wiley, New York, 1990).
13. R. Becker and W. Doring, *Ann. Phys.* **24**, 719 (1935); F. F. Abraham, *Homogeneous Nucleation Theory* (Academic Press, New York, 1974), chap. 5.
14. H. Shin et al., *J. Mater. Res.* **10**, 692 (1995); E. B. Slamovich and I. A. Aksay, *J. Am. Ceram. Soc.* **79**, 239 (1996).
15. S. Mann, in *Biomimetic Materials Chemistry*, S. Mann, Ed. (VCH Press, New York, 1996), pp. 1–40; B. R. Heywood, *ibid.*, pp. 143–174; F. C. Meldrum and J. Fendler, *ibid.*, pp. 175–220.
16. S. Mann, *Nature* **332**, 119 (1988).
17. The SAM approach for metal substrates involves the use of organothiol rather than chlorosilane surfactants.
18. A. Kumar and G. M. Whitesides, *Appl. Phys. Lett.* **63**, 2002 (1993); A. Kumar, H. A. Biebuyck, G. M. Whitesides, *Langmuir* **10**, 1498 (1994).
19. B. J. Tarasevich, P. C. Rieke, J. Liu, *Chem. Mater.* **8**, 292 (1996); P. C. Rieke et al., *Langmuir* **10**, 619 (1994).
20. M. R. De Guire et al., *SPIE Proc.*, in press.
21. R. J. Collins, H. Shin, M. R. De Guire, C. N. Sukenik, A. H. Heuer, unpublished results.
22. E. Kim, Y. Xia, G. M. Whitesides, *Nature* **376**, 581 (1995).
23. C. T. Kresge et al., *Nature* **359**, 710 (1992); J. S. Beck et al., *J. Am. Chem. Soc.* **114**, 10834 (1992).
24. D. M. Antonelli and J. Y. Ying, *Angew. Chem. Int. Ed. Engl.* **34**, 2014 (1995).

25. P. V. Braun, P. Osenar, S. I. Strupp, *Nature* **380**, 325 (1996).
26. A. Monnier *et al.*, *Science* **261**, 1299 (1993); A. Firouzi *et al.*, *ibid.* **267**, 1138 (1995); C. H. Chen, S. L. Burkett, H. X. Li, M. E. Davis, *Microporous Mater.* **2**, 27 (1993).
27. H. Yang *et al.*, *Nature* **379**, 703 (1996).
28. S. Manne *et al.*, *Langmuir* **10**, 4409 (1994); _____ and H. Gaub, *Science* **270**, 1480 (1995).
29. The procedure involves dissolving TEOS liquid in an aqueous solution of CTAC and hydrochloric acid. Typical molar ratios are 1 TEOS:2 CTAC:9.2 HCl:1000 H₂O. Under these solution conditions, mesoscopic silica films spontaneously grow onto substrates in contact with the liquid.
30. Under similar conditions, freestanding mesostructured silica films can also be grown at the air/water interfaces [H. Yang *et al.*, *Nature* **381**, 589 (1996); and work at Princeton University by N. Nakagawa *et al.*, unpublished results].
31. To obtain these images, we used a method described in (28) and (32) that uses electrical double layer repulsive forces to image the charge distribution of an adsorbed layer on the sample. The images of the outer layer of the reacting mesostructured film were obtained by immersing the imaging tip and substrate in the reacting mixture and, once sufficient time was allowed for thermal and mechanical equilibration, setting the imaging setpoint in the repulsive precontact region. In this way, the tip is held ~1 nm above the reacting surface and the scanning motion of the AFM produces a topological map of charge density.
32. T. J. Senden, C. J. Drummond, P. Kekicheff, *Langmuir* **10**, 358 (1994).
33. After 10 hours of reaction, in situ AFM images are difficult to obtain because of the appreciable growth of mesostructured silica on the top surface of the AFM flow cell and cantilever spring. The presence and irregular nature of both of these films disturb the reflection of the laser light beam used to monitor spring deflection.
34. AFM studies on systems containing only surfactant, with no TEOS, reveal the presence of several layers of adsorbed surfactant tubules. Three-dimensional "multilayer" features have been imaged with the microscope, and as many as three "steplike" features are observed in the repulsive portion of the force-distance curve near the substrate (M. Trau *et al.*, in preparation). The existence of such supramolecular surfactant structures in the absence of TEOS suggests a sequential reaction mechanism involving surfactant self-assembly followed by inorganic condensation.
35. Y. Gao, J. Du, T. Gu, *J. Chem. Soc. Faraday Trans. 1* **83**, 2671 (1987); B.-Y. Zhu and T. Gu, *ibid.* **85**, 3813 (1989); T. Gu and Z. Huang, *Colloids Surf.* **40**, 71 (1989); J. Leimbach and J. S. H. Rupprecht, *ibid.* **94**, 1 (1995).
36. W. Z. Helfrich, *Naturforschung* **28C**, 693 (1973).
37. S. M. Gruner, *J. Phys. Chem.* **93**, 7562 (1989); R. P. Rand *et al.*, *Biochemistry* **29**, 76 (1990).
38. We observed +18% strain in the film grown in the nonequilibrium condition, in the case where the solution is confined in a thin film geometry by a wrap. We found that the film grows about an order of magnitude faster in this condition. A striking feature of our data is that there is a large change in the Bragg peak position as these films dry that corresponds to large changes in the film lattice constant and strain. For example, the degree of hexagonal strain varies from +18% while wet to +2% a few hours after removal from solution, and finally -7% several days later when they are dry. In this process, the lateral spacings of the film increased by 2% upon drying and finally by 5% after a few days. This implies that the 25% change in *a/b* ratio of the film upon drying is largely due to a change in the vertical lattice spacings due to drying shrinkage in the normal direction.
39. This work was supported by the U.S. Army Research Office (grant DAAH04-95-1-0102) and MRSEC program of the NSF (DMR-940032). We thank D. M. Dabbs for useful discussions and help in the manuscript preparation and Digital Instruments for technical support.

Synthesis of Novel Thin-Film Materials by Pulsed Laser Deposition

Douglas H. Lowndes, D. B. Geohegan, A. A. Puretzky, D. P. Norton, C. M. Rouleau

Pulsed laser deposition (PLD) is a conceptually and experimentally simple yet highly versatile tool for thin-film and multilayer research. Its advantages for the film growth of oxides and other chemically complex materials include stoichiometric transfer, growth from an energetic beam, reactive deposition, and inherent simplicity for the growth of multilayered structures. With the use of PLD, artificially layered materials and metastable phases have been created and their properties varied by control of the layer thicknesses. In situ monitoring techniques have provided information about the role of energetic species in the formation of ultrahard phases and in the doping of semiconductors. Cluster-assembled nanocrystalline and composite films offer opportunities to control and produce new combinations of properties with PLD.

The first PLD experiment was carried out more than 30 years ago, shortly after the invention of the pulsed ruby laser (1). However, it was only during the past decade that PLD received extensive experimental development and came into widespread use for film-growth research. The impetus was the discovery that high-quality high-temperature (high-*T_c*) superconductor (HTS) films can be grown in a low-pressure oxygen environment by PLD

without the need for further processing (2). This discovery opened the field of oxide ceramic film growth and research to PLD; in turn, PLD has invigorated and enriched the oxide field. During the past 9 years, PLD's advantages for the deposition of oxides and other complex materials have been used to grow films with an enormous variety of properties, including ferroelectrics, ferrites, amorphous diamond and other ultrahard phases, biocompatible and tribological coatings, polymers, compound semiconductors, and nanocrystalline materials (3).

This article describes the ablation process and its characteristic advantages and limitations for film deposition. Three

themes in contemporary PLD research then are examined: (i) the creation of artificial structures and metastable phases and the systematic variation of their properties, (ii) information about the role of energetic ablated species in the formation of ultrahard phases and in the doping of semiconductors, and (iii) emerging opportunities in the synthesis of nanocrystalline and composite thin-film materials with PLD.

Pulsed Laser Ablation

Although the underlying ablation process is complex, PLD is conceptually and experimentally simple. An ultraviolet (UV) pulsed laser beam (pulse duration, 10 to 50 ns) is focused with an energy density E_d of 1 to 5 J/cm² onto a rotating polycrystalline target (Fig. 1). Several events occur during the laser pulse: rapid heating and vaporization of the target; increasing absorption by the vapor until breakdown occurs to form a dense plasma; and absorption of the remainder of the laser pulse to heat and accelerate the plasma, which contains neutral atoms, molecules, and ions, in both ground and excited states, as well as energetic electrons. The atoms and ions undergo collisions in the high-density region near the target (the Knudsen layer, which is a few hundred micrometers thick) to create a highly directional expansion perpendicular to the target surface with initial velocities $\geq 10^6$ cm/s. If ablation is carried out in a low-pressure reactive gas such as oxygen, simple oxide molecules are also formed in the expanding ablation beam. In an ambient gas, a shock front results from collisions between the expanding plasma and the gas molecules (Fig. 2). This front propagates with gradu-

D. H. Lowndes, D. B. Geohegan, D. P. Norton, and C. M. Rouleau are in the Solid State Division, Oak Ridge National Laboratory, Post Office Box 2008, Oak Ridge, TN 37831-6056, USA. A. A. Puretzky is at the Institute of Spectroscopy, Russian Academy of Sciences, Troitsk, Russia.